Reliability Analysis of Corroded RC Structures Integrating Hybrid Bayesian Network

Hongyuan Guo[1], You Dong[1], Dan M.Frangopol[2]

1, Dept. of Civil and Environmental Engineering, Hong Kong Polytechnic University, Hong Kong SPR, China

2, Dept. of Civil and Environmental Engineering, Lehigh University, Bethlehem, PA, USA

Abstract: The performance of RC structures might deteriorate with time due to environmental stressors (e.g., chloride ingress and concrete carbonation), compromising structural safety and social sustainability. Many studies have shown that probabilistic methods are necessary for the performance and reliability assessment of deteriorating RC structures, considering the uncertainty of environmental changes and material properties. However, most previous studies only considered the reliability prediction of deteriorated RC structures at the design stage. Recent studies proved that the inspection results could significantly reduce the uncertainties in the life cycle assessment of RC structures. Thus, a hybrid Bayesian network (HBN)-based reliability calculation framework is developed by integrating durability assessment and mechanical assessment of deteriorated RC structures. Experimentally validated 2D chloride transport models and analytical models are used to calculate the durability and mechanical properties of RC beams. Also, different dynamic Bayesian networks are combined into one HBN to perform Bayesian inference. In addition, a low-discrepancy pseudo-random sequence is utilized in building the HBN to improve the efficiency and accuracy of the modeling. Finally, to demonstrate the performance and detection results of the framework in the life-cycle reliability analysis of RC structures, the proposed framework is applied to an illustrative case.

1. Introduction

To date, Bayesian methods have been widely used for probabilistic inference of reinforced concrete (RC) structures by updating data collected from monitoring systems or field inspections [1]. However, due to the complexity of actual RC structures, updating and inferring parameters based on traditional Bayesian methods would be challenging for practical engineering. Therefore, to update the reliability assessment of RC structures by probabilistic detection data, a graphical model called Bayesian Network (BN) has been widely used [2,3]. Tran *et al.* [4–6] also used static BN (SBN) to determine the parameters and uncertainties of the corrosion initiation probability of RC structures deteriorated under chloride attack, considering the corrosion of steel reinforcement due to chloride ingress.

However, SBN cannot take into account the time dependencies of the parameters associated with the aging of the concrete, the surface chloride concentration, the loading, etc. Consequently, dynamic Bayesian networks (DBNs) have been proposed to handle BN updates and inference under multiple time slices [7,8]. For example, Guo and Dong [9] developed a generic DBN framework for assessing the durability of RC structures exposed to the marine atmosphere. Taking into account the uncertainty of climate change and chloride transport, such a framework can investigate the effect of the investigated concrete cracks on the durability of the RC structures. Nevertheless, this DBN framework focuses only on the durability assessment of RC structures, not their mechanical properties. However, limited to the existing DBN technology, the complex analysis of the life cycle reliability of RC structures will become a challenge because a large number of relevant parameters will increase the computational burden exponentially. To overcome the drawbacks of existing BNs related studies, this study proposed a comprehensive Bayesian network-based framework to achieve life cycle reliability analysis for RC structures in long-term environmental action.

2. Hybrid Bayesian Network for Reliability Assessment

2.1. General DBN for reliability assessment

The proposed reliability assessment framework for RC structures consists of three main phases: durability, mechanics, and reliability assessment. In the first phase, the main tasks are to capture the corrosion rate i_{corr}, the reinforcement radius reduction Δr, and so on [9]. Next, in the second phase, corroded RC beams are investigated, where the flexural and shear capacity of each section is analyzed to consider the spatial effects of chloride-induced reinforcement corrosion [10]. Furthermore, the equivalent loading capacity of RC beams could be obtained by the minimum value of P_{Mu} and P_{Vu}. Then, taking into account the external load distribution, the performance function g_{u} can be captured, where the probability of $g_{\mathrm{u}} \leqslant 0$ indicates the failure probability [10].

According to previous studies [10–12], the critical variables (e.g., the chloride content of concrete surface c_{surf}, chloride diffusion coefficient D_{cref}, and cross-sectional areas of tension bars at different section such as $A_1{}^t$, $A_2{}^t$, etc.) can be extracted to form a giant DBN, as illustrated in Fig. 1. DBN generally contains a series of T time-slice BNs and a set of nodes (i.e., random variables) $X_{1:n_{bn}}^i = \{X_1^i, \ldots, X_{n_{bn}}^i\}, i = 1, \ldots, T$ at different time instants and its joint probability distribution of all nodes over time T is marked as $P\left(X_{1:n_{bn}}^{1:T}\right)$ [8,13]:

$$P\left(X_{1:n_{bn}}^{1:T}\right) = \prod_{i=1}^{T-1} P\left(X_{1:n_{bn}}^{i+1} \mid X_{1:n_{bn}}^{i}\right) \tag{1}$$

where $P\left(X_{1:n_{bn}}^{i+1} | X_{1:n_{bn}}^{i}\right)$ denotes the conditional probability distribution at the i+1-th time slice given the probability information of nodes at the i-th time slice.

In addition, all continuous nodes must be discretized into discrete nodes to perform exact inference. Meanwhile, the conditional probability distribution of each node is transformed into conditional probability mass functions (PMFs), expressed by conditional probability tables (CPTs). Representative samples based on performance evaluation models of RC structures need to be selected to construct CPTs for each node, whose main algorithms refer to [11]. In practical BN inference, a frontier algorithm is used to reduce the difficulty of DBN inference [8].

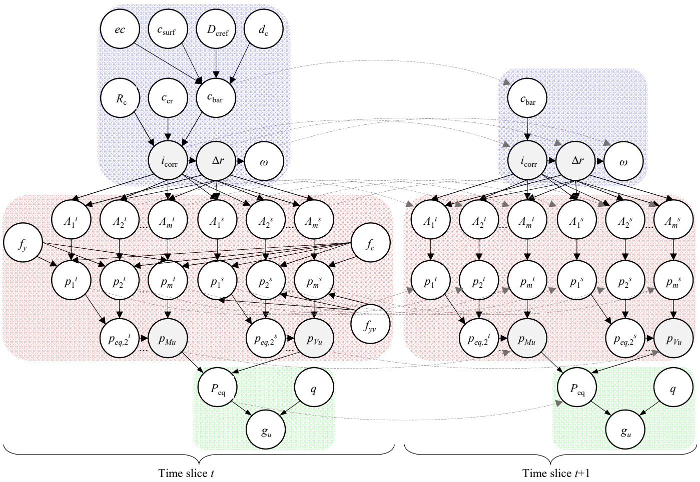

Fig. 1 DBN for reliability estimation of RC structures subjected to chloride ingression (Blue, red, and green zone denote the durability, mechanics, and reliability assessments, respectively)

2.2. HBN: simplification of DBN

Although existing strategies could simplify the difficulty in DBN modeling [2,3], the direct implementation of such a DBN framework is computationally challenging due to the large number of parameters associated with different models. Thus, a Hybrid Bayesian Network (HBN) is proposed in this study, as shown in Fig. 2. Each node in the HBN denotes a sub-DBN and its output nodes. These variables are shared nodes for adjacent sub-DBNs. Given the inspection results of corrosion-induced crack width ω in the DBNs of 'i_{corr}' and 'Δr', the PMFs of the nodes of i_{corr} and Δr can be updated. Then, the nodes of i_{corr} and Δr act as inspection nodes in the DBNs of 'P_{Mu}' and 'P_{Vu}'. Meanwhile, the updated PMFs of i_{corr} and Δr become posterior distributions, i.e., soft or uncertain evidence [14,15]. The above procedure is also applied to nodes P_{Mu} and P_{Vu} for reliability update and evaluation. Besides, an effective strategy is to perform soft evidence-based BN inference to achieve the above process. The node discretization, the CPT computation, and the inference algorithms of the HBN are identical to those of the DBN in Section 2.1.

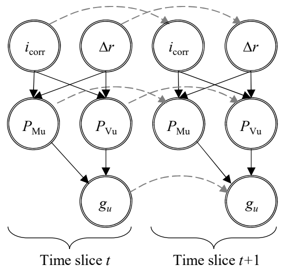

Fig. 2 HBN for reliability assessment of RC structures subjected to chloride ingression

3. Reliability assessment models

3.1. Durability assessment

Realistic modeling of environmental parameters, such as temperature (T), relative humidity (RH), and chloride deposition, is essential for the durability assessment. Therefore, an environmental model is employed including seasonal f_{sea} and daily variability f_{dai}, an increasing trend f_{inc}, and a random noise ξ, as shown in Eq.(2) [16,17].

$$f(ec,t) = f_{\text{sea}}(t) + f_{\text{dai}}(t) + f_{\text{inc}}(ec,t) + \xi \tag{2}$$

where t is the current time (day); and ec is the characteristic value of exposure conditions. Given the boundary conditions provided by Eq.(2), the chloride ingress process into concrete could be simulated by the following equation [17]:

$$\frac{\partial C_{\text{fc}}}{\partial t} = D_c^*\left(\frac{\partial^2 C_{\text{fc}}}{\partial x^2} + \frac{\partial^2 C_{\text{fc}}}{\partial y^2}\right) + D_h^*\left(\frac{\partial}{\partial x}\left(C_{\text{fc}}\frac{\partial h_{\text{RH}}}{\partial x}\right) + \frac{\partial}{\partial y}\left(C_{\text{fc}}\frac{\partial h_{\text{RH}}}{\partial y}\right)\right) \tag{3}$$

where C_{fc} is free chloride content (kg/m^3 of pore solution); and D_{c}^* and D_{h}^* are the apparent diffusion coefficients of chlorides and moisture (m^2/s), respectively. In this stud, Eq. (3) is solved by finite difference method (FDM) to capture the chloride content of the reinforcement surface c_{bar} [18]. When c_{bar} is beyond critical value c_{cr}, reinforcement corrosion start, and the corrosion rate is assessed by [19]:

$$\begin{aligned} \ln\left[1.08 i_{\text{corr}}(t)\right] &= 7.89 + 0.7771 \cdot \ln(1.69 c_{\text{bar}}) \\ &- 3006/T_{con} - 0.000116 \cdot R_c + 2.24 t_{\text{corr}}^{-0.215} + \varpi \end{aligned} \tag{4}$$

where $i_{\text{corr}}(t)$ is the corrosion current density (μA/cm^2); T_{con} (K) and R_{con} (Ohms) are the temperature and resistance within the concrete; t_{corr} (year) is the time after corrosion; and ϖ is a random variable N(0, 0.3312) [16]. Besides, the corrosion-induced crack width ω (mm) is evaluated by an empirical model [20]:

$$
\begin{aligned}
&\omega(t)=0.0575\cdot\left[\pi d_0^2-A_{ave}(t)-\Delta A_{s0}\right],\\
&A_{ave}(t)=\pi\left[d_0-2\cdot\int_0^t 0.0116 i_{\mathrm{corr}}(t)\,\mathrm{d}t\right]^2,\\
&\Delta A_{s0}=\pi d_0^2\left\{1-\left[1-2/d_0\left(7.53+9.32c_{\mathrm{t}}/d_0\right)10^{-3}\right]^2\right\}
\end{aligned}
\tag{5}
$$

where d_0 is the initial diameter of steel bars; and $A_{\mathrm{ave}}(t)$ is the average residual cross-sectional area of the corroded steel bar;.ΔA_{s0} is the reduction of the cross-sectional area once concrete cracks; and c_t (mm) is the thickness of the concrete cover.

3.2. Mechanical capacity assessment

A simply supported corroded RC beam is investigated. The total and effective length, cover thickness, and stirrup spacing of this beam are denoted as l, l_{eft}, c, and s_{v}, respectively. Considering spatial variability in the mechanical capacities of corroded RC beams, the beams are separated into m zones concerning the spatial effects of non-uniform corrosion [21,22]. The corrosion non-uniformity factor R quantifies the non-uniform reinforcement corrosion following the Gumbel distribution [10,17,21].

$$
R(t)=A_{\mathrm{ave}}(t)/A_{\mathrm{min}}(t) \tag{6}
$$

Based on the assumptions of planar sections and perfect bond behavior, their flexural capacities $M_{u,k}(t)$ and shear bearing capacity $V_k(t)$ at each zone can be calculated by Eqs.(7) and (8), respectively [10,21,23].

$$
M_{u,k}(t)=f_{\mathrm{y0}}\cdot A_k^t(t)\cdot\left[h_0-0.5f_{\mathrm{y0}}\cdot A_k^t(t)/\left(b\cdot f_{\mathrm{c}}\right)\right] \tag{7}
$$

$$
V_k(t)=1.75/\left(\lambda_s+1\right)\cdot f_{\mathrm{t}}bh_0+f_{\mathrm{yv0}}\cdot h_0/s_{\mathrm{v}}\sum_{w=1}^{n_{\mathrm{sv}}}A_{\mathrm{min},k,w}^{s}(t) \tag{8}
$$

where b, h, and h_0 are the cross-sectional width, total height, and effective height, respectively; f_{c} is the concrete compressive strength (MPa); f_{y0} is the yield strength of uncorroded tension bars; $A^t{}_k(t)$ is the equivalent cross-sectional area of tension bars in the k-th zone [21]; f_t is the concrete tensile strength; λ_{s} is the shear-to-span ratio; f_{yv0} is the yield strength of uncorroded stirrup bars; n_{sv} is the number of stirrup legs; $A^t{}_k(t)$ is the equivalent cross-sectional area sum of stirrup bars in the k-th zone; and $A_{min,k,w}^{s}(t)$ (k=1, 2, ..., m; w= 1,2, ..., n_{sv}) is the minimum cross-sectional area (mm^2) of the w-th stirrup bar of the k-th zone.

3.3. Time-dependent reliability assessment

To implement time-dependent reliability analysis, the performance functions $g(\boldsymbol{\theta}, t)$ is built given ultimate limit state (ULS), and corresponding to critical load P_{u}:

$$
g_u(\boldsymbol{\theta},t)=P_u(\boldsymbol{\theta},t)-S(\boldsymbol{\theta},t) \tag{9}
$$

in which $\boldsymbol{\theta}$ is the vector of all input variables; and $P_{\mathrm{u}}(\boldsymbol{\theta}, t)$ and $S(\boldsymbol{\theta}, t)$ are the ultimate capacities and external load at a given instant t and $\boldsymbol{\theta}$, respectively. In addition, considering the first passage issue, the time-dependent failure probability $p_{f,u}(t)$ could be described as the probability that $g_{\mathrm{u}}(\boldsymbol{\theta}, t)$ reaches the critical value within an investigated time interval [0,t], i.e., Eq.(10). In BN based reliability, $p_{f,u}(t)$ is computed by the PMF of binary distributed $g_{\mathrm{u}}(\boldsymbol{\theta}, t)$.

$$
p_{f,u}(t)=\Pr\left\{g_u(\boldsymbol{\theta},\tau)\le 0,\tau\in[0,t]\right\} \tag{10}
$$

4. Numerical case

To illustrate and study the efficiency of the developed framework, it is assumed that a simply supported RC beam with a cross-section of 150 × 300 mm has been located on the west coast of the Yellow Sea since 2010 [17]. The parameters of the beam geometry and reinforcement layout are listed in Table 1. Furthermore, Table 2 lists the distribution types and parameters of isolated parent nodes in all sub-BNs.

Table 1 Geometry parameters and reinforcement of RC beams

Parameters	Value	Parameters	Value
Total length l	5400 mm	Effective length l_{eft}	5000 mm
Effective section height h_0	275 mm	Stirrup spacing s_v	250 mm
Section width b	150 mm	Number of tension bars n_t	3
Initial diameter of tension bars d_{t0}	20 mm	Number of compression bars $n_{t'}$	2
Initial diameter of compression bars $d_{t'0}$	12 mm	Number of stirrup bars n_{sv}	2
Initial diameter of stirrup bars d_{sv0}	6 mm	Number of zones m	20

Table 2 Distribution types and values of parent nodes in HBN

Parameters	Distribution	μ	δ	Ref
Baseline of chloride deposition c_{surf0} (wt% of cement)	Gaussian	0.65	0.1	[17]
Reference coefficient of chloride diffusion D_0(10^{-11} m^2/s)	Lognormal	1.6	0.1	[24]
Cover thickness c (mm)	Gaussian	25	0.05	[25]
Critical chloride content c_{cr} (wt% of cement)	Lognormal	0.4	0.1	[26]
Resistance of concrete cover R_c(kΩ)	Lognormal	25	0.1	[16]
Compressive strength of concrete f_c (MPa)	Gaussian	25	0.15	[26]
Yield strength of longitudinal bars (MPa)	Gaussian	360	0.05	[27]
Yield strength of stirrup bars (MPa)	Gaussian	220	0.05	[28]

Note: μ and δ are the lower and upper bounds for the uniform distribution value, while μ and δ are the mean and coefficient of variation (COV) for other distributions.

4.1. HBN establishment

The priori information of all nodes in the HBNs needs to be determined through representative samples. Thus, the good lattice points-based point selection method is employed to generate 610 representative samples based on the distribution information in Table 2 [11,29]. To reduce the analysis burden, the number of time slices, nodes, and links in HBN is appropriately reduced. Consistent with previous studies [11], the time intervals and the number of time slices are preset to 3 years and 18, and the number of discrete statuses for each node is set to 8 except for node g_u. Since RC beams are separated into m zones, there are a large number of random variables associated with the cross-sectional area of the corroded reinforcement (A_k^t and A_k^s, k=1, 2, ..., m). Thus, sensitivity analysis is implemented to investigate the contributions of each spatial zone to the mechanical performance of RC beams. As illustrated in Fig. 3, the probability of ULS occurrence in each zone is calculated based on 610 representative samples over 50 years. As shown, flexural failure events are concentrated at the mid-span of the RC beam. In contrast, the shear damage events are concentrated near the supports of the RC beam, which is consistent with mechanical behavior [30,31].

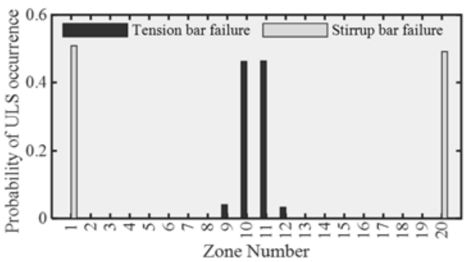

Fig. 3 Probability distribution of ULS occurrence caused by non-uniform corrosion over 50 years

Besides, according to the sensitivity results, the 9th to 12th zones (i.e., A_9^t to A_{12}^t) are of interest for flexural failure, and the 1st and 20th zones (i.e., A_1^s and A_{20}^s) are of interest for shear failure. All nodes in HBNs are discretized into discrete nodes, and their CPTs are computed accordingly [11].

4.2. Inference results

The width ω of corrosion-induced concrete crack could be detected at several inspection instants (e.g., 3, 12, 21, 30, and 39 years). Also, possible inspection results of corrosion-induced concrete crack width ω (mm) are assumed: $\omega_1 \in [0, 0.1]$, $\omega_2 \in [0.2, 0.3]$, and $\omega_3 \in [0.5, 0.6]$ [11]. The HBN is used to infer critical parameters of the structural performance of RC beams subjected to different inspections. For the sake of the comparisons, the mean of discrete nodes is used and calculated by Eq. (11) [11].

$$E(x) = 0.5 \cdot \sum_{k=1}^{n_x} \left(d_k + d_{k+1}\right) \cdot P_x(k) \tag{11}$$

in which $[d_1, d_2, \ldots, d_{n_x+1}]$ is the discretization scheme of the target node x; and $P_x(k)$ is the PMF of x at its k-th interval. Fig. 4 displays the mean values of P_{Mu} and P_{Vu} under different inspection results, where the mean value of P_{Mu} over time is higher than P_{Vu}. As shown, the mean values keep decreasing with time, and those of P_{Mu} and P_{Vu} with the 3rd year inspection of ω_2 decrease the fastest among all scenarios, with maximum reductions of 9% for P_{Mu} and P_{Vu} compared to no inspection. Besides, for the 21st-year inspection, the mean values of P_{Mu} and P_{Vu} decreased much more slowly than in other scenarios, with a maximum increase of 7% and 5% for P_{Mu} and P_{Vu} compared to no inspection. The above results indicate that early inspection of moderate-width cracks significantly reduces the mean value of the load capacity.

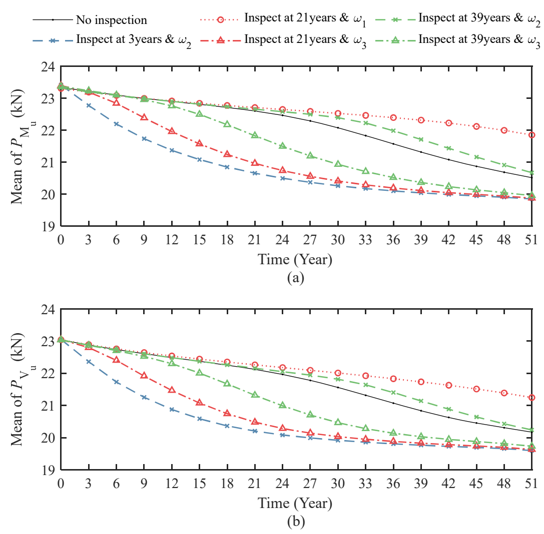

Fig. 4 Mean of P_{Mu} and P_{Vu} subject to different inspection results: (a) P_{Mu}; and (b) P_{Vu}

In addition, Fig. 5 presents that the effects of inspection results on $p_{f,\mathrm{u}}$ are significant. For instance, given the 3rd year inspection of ω_2 and 12th year inspection of ω_3, $p_{f,u}$ is maximum 2.11×10^5% and 1.67×10^5% higher than no inspection. Besides, given the inspections of crack width, $p_{f,\mathrm{u}}$ decreases with the inspection time. For instance, $p_{f,\mathrm{u}}$ with a 3rd-year inspection of ω_1 is maximum 22% lower than no inspection, and $p_{f,\mathrm{u}}$ with a 30th-year inspection of ω_1 is maximum 95% lower than no inspection. Besides, compared to no inspection, $p_{f,\mathrm{u}}$ with the 12th-year inspection of ω_2 is maximum 1.6×10^4 % higher, while $p_{f,\mathrm{u}}$ with the 30th-year inspection of ω_2 is maximum 73% higher.

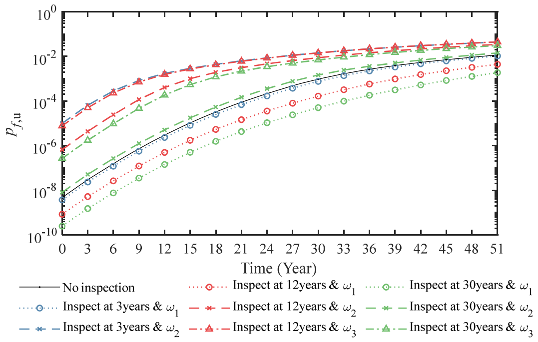

Fig. 5 Time-dependent failure probability $p_{f,u}$ of the beam considering on ULS and different inspection results

5. Conclusion

This study proposed an HBN-based framework for the reliability estimation of corroded RC structures subject to chloride ingress. The reliability analysis for RC beams under marine atmospheric environment is utilized to illustrate the proposed framework, and the following conclusion can be drawn:

(1) Inference results of MBN prove that the proposed framework could use the results of inspections to update the probabilistic distribution of mechanical capacity and performance functions over time.

(2) For load capacities, results indicate that early inspection of medium-width cracks decreases the mean values of load capacities by about 9%. In comparison, the small-width cracks raise the mean values of load capacities by about 5 to 6%.

(3) Considering ultimate limit states, an early inspection of the high level of corrosion-induced cracks might dramatically increase the failure probability by about 2×10^{5}%, and later inspection of small corrosion-induced cracks might decrease the failure probability by about 95%

In summary, it is practical to use the proposed HBN framework for the reliability assessment of RC structures developed.

References:

[1] Estes AC, Frangopol DM. Updating Bridge Reliability Based on Bridge Management Systems Visual Inspection Results. J Bridg Eng 2003;8:374–82. https://doi.org/10.1061/(asce)1084-0702(2003)8:6(374).

[2] Straub D, Der Kiureghian A. Bayesian Network Enhanced with Structural Reliability Methods: Application. J Eng Mech 2010;136:1259–70. https://doi.org/10.1061/(asce)em.1943-7889.0000170.

[3] Straub D, Der Kiureghian A. Bayesian Network Enhanced with Structural Reliability Methods: Methodology. J Eng Mech 2010;136:1248–58. https://doi.org/10.1061/(asce)em.1943-7889.0000173.

[4] Tran TB, Bastidas-Arteaga E, Schoefs F. Improved Bayesian network configurations for probabilistic identification of degradation mechanisms: application to chloride ingress. Struct Infrastruct Eng 2016;12:1162–76. https://doi.org/10.1080/15732479.2015.1086387.

[5] Tran TB, Bastidas-Arteaga E, Schoefs F. Improved Bayesian network configurations for random variable identification of concrete chlorination models. Mater Struct Constr 2016;49:4705–18. https://doi.org/10.1617/s11527-016-0818-4.

[6] Tran TB, Bastidas-Arteaga E, Schoefs F, Bonnet S. A Bayesian network framework for statistical characterisation of model parameters from accelerated tests: application to chloride ingress into concrete. Struct Infrastruct Eng 2018;14:580–93. https://doi.org/10.1080/15732479.2017.1377737.

[7] Tran TB, Bastidas-Arteaga E, Aoues Y. A Dynamic Bayesian Network framework for spatial deterioration modelling and reliability updating of timber structures subjected to decay. Eng Struct 2020;209:110301. https://doi.org/10.1016/j.engstruct.2020.110301.

[8] Murphy KP. Dynamic Bayesian Networks: Representation, Inference and Learning. University of California, Berkeley, 2002.

[9] Zacchei E, Bastidas-Arteaga E. Multifactorial Chloride Ingress Model for Reinforced Concrete Structures Subjected to Unsaturated Conditions. Buildings 2022;12. https://doi.org/10.3390/buildings12020107.

[10] Guo HY, Dong Y, Gu XL. Two-step translation method for time-dependent reliability of structures

subject to both continuous deterioration and sudden events. Eng Struct 2020;225:111291. https://doi.org/10.1016/j.engstruct.2020.111291.
[11] Guo HY, Dong Y. Dynamic Bayesian network for durability of reinforced concrete structures in long-term environmental exposures. Eng Fail Anal 2022;142:106821. https://doi.org/10.1016/j.engfailanal.2022.106821.
[12] Guo HY, Dong Y, Bastidas-Arteaga E, Gu XL. Probabilistic failure analysis, performance assessment, and sensitivity analysis of corroded reinforced concrete structures. Eng Fail Anal 2021;124:105328. https://doi.org/10.1016/j.engfailanal.2021.105328.
[13] Hackl J, Kohler J. Reliability assessment of deteriorating reinforced concrete structures by representing the coupled effect of corrosion initiation and progression by Bayesian networks. Struct Saf 2016;62:12–23. https://doi.org/10.1016/j.strusafe.2016.05.005.
[14] Nagarajan R, Scutari M, Lèbre S. Bayesian Networks in R. 2013. https://doi.org/10.1007/978-1-4614-6446-4.
[15] Scutari M, Denis J-B. Bayesian Networks with examples in R. 2014. https://doi.org/10.1201/b17065.
[16] Flint MM, Baker JW, Billington SL. A modular framework for performance-based durability engineering: From exposure to impacts. Struct Saf 2014;50:78–93. https://doi.org/10.1016/j.strusafe.2014.03.003.
[17] Guo HY, Dong Y, Gu XL. Durability assessment of reinforced concrete structures considering global warming: A performance-based engineering and experimental approach. Constr Build Mater 2020;233:117251. https://doi.org/10.1016/j.conbuildmat.2019.117251.
[18] Carnahan B, Luther HA. Applied numerical methods. New York: John Wiley & Sons; 1969.
[19] Liu T, Weyers RW. Modeling the dynamic corrosion process in chloride contaminated concrete structures. Cem Concr Res 1998;28:365–79. https://doi.org/10.1016/S0008-8846(98)00259-2.
[20] Vidal T, Castel A, François R. Analyzing crack width to predict corrosion in reinforced concrete. Cem Concr Res 2004;34:165–74. https://doi.org/10.1016/S0008-8846(03)00246-1.
[21] Gu XL, Guo HY, Zhou B Bin, Zhang WP, Jiang C. Corrosion non-uniformity of steel bars and reliability of corroded RC beams. Eng Struct 2018;167:188–202. https://doi.org/10.1016/j.engstruct.2018.04.020.
[22] Zhao YX, Karimi AR, Wong HS, Hu BY, Buenfeld NR, Jin WL. Comparison of uniform and non-uniform corrosion induced damage in reinforced concrete based on a Gaussian description of the corrosion layer. Corros Sci 2011;53:2803–14. https://doi.org/10.1016/j.corsci.2011.05.017.
[23] Stewart MG. Mechanical behaviour of pitting corrosion of flexural and shear reinforcement and its effect on structural reliability of corroding RC beams. Struct Saf 2009;31:19–30. https://doi.org/10.1016/j.strusafe.2007.12.001.
[24] Val D V., Melchers RE. Reliability of deteriorating RC slab bridges. J Struct Eng 1997;123:1638–44. https://doi.org/10.1061/(ASCE)0733-9445(1997)123:12(1638).
[25] Tu B, Dong Y, Fang Z. Time-Dependent Reliability and Redundancy of Corroded Prestressed Concrete Bridges at Material, Component, and System Levels. J Bridg Eng 2019;24. https://doi.org/10.1061/(asce)be.1943-5592.0001461.
[26] Bastidas-Arteaga E, Schoefs F, Stewart MG, Wang X. Influence of global warming on durability of corroding RC structures: A probabilistic approach. Eng Struct 2013;51:259–66. https://doi.org/10.1016/j.engstruct.2013.01.006.
[27] Ye ZW, Zhang WP, Gu XL. Deterioration of shear behavior of corroded reinforced concrete beams. Eng Struct 2018;168:708–20. https://doi.org/10.1016/j.engstruct.2018.05.023.
[28] Darmawan MS, Stewart MG. Spatial time-dependent reliability analysis of corroding pretensioned prestressed concrete bridge girders. Struct Saf 2007;29:16–31. https://doi.org/10.1016/j.strusafe.2005.11.002.
[29] Guo HY, Dong Y, Gardoni P. Efficient subset simulation for rare-event integrating point-evolution kernel density and adaptive polynomial chaos kriging. Mech Syst Signal Process 2022;169:108762. https://doi.org/10.1016/j.ymssp.2021.108762.
[30] Hajializadeh D, Stewart MG, Enright B, O'Brien EJ. Spatial time-dependent reliability analysis of reinforced concrete slab bridges subject to realistic traffic loading. Struct Infrastruct Eng 2015:1–16. https://doi.org/10.1080/15732479.2015.1086385.
[31] Stewart MG, Al-Harthy A. Pitting corrosion and structural reliability of corroding RC structures: Experimental data and probabilistic analysis. Reliab Eng Syst Saf 2008;93:373–82. https://doi.org/10.1016/j.ress.2006.12.013.